A Targeted RNAi Screen Identifies Endocytic Trafficking Factors That Control GLP-1 Receptor Signaling in Pancreatic β-Cells

Buenaventura, Teresa; Kanda, Nisha; Douzenis, Phoebe C; Jones, Ben; Bloom, Stephen R; Chabosseau, Pauline; Corrêa, Ivan R (Jr); Bosco, Domenico; Piemonti, Lorenzo; Marchetti, Piero; Johnson, Paul R; Shapiro, A M James; Rutter, Guy Allen; Tomas Catala, Alejandra Del Don

How to cite

BUENAVENTURA, Teresa et al. A Targeted RNAi Screen Identifies Endocytic Trafficking Factors That Control GLP-1 Receptor Signaling in Pancreatic β-Cells. In: Diabetes, 2018, vol. 67, n° 3, p. 385–399. doi: 10.2337/db17-0639

This publication URL: https://archive-ouverte.unige.ch/unige:116918

Publication DOI: 10.2337/db17-0639

A Targeted RNAi Screen Identifies Endocytic Trafficking Factors That Control GLP-1 Receptor Signaling in Pancreatic β-Cells

Teresa Buenaventura,[1] Nisha Kanda,[1] Phoebe C. Douzenis,[1] Ben Jones,[2] Stephen R. Bloom,[2] Pauline Chabosseau,[1] Ivan R. Corrêa Jr.,[3] Domenico Bosco,[4] Lorenzo Piemonti,[5,6] Piero Marchetti,[7] Paul R. Johnson,[8] A.M. James Shapiro,[9] Guy A. Rutter,[1] and Alejandra Tomas[1]

Diabetes 2018;67:385–399 | https://doi.org/10.2337/db17-0639

The glucagon-like peptide 1 (GLP-1) receptor (GLP-1R) is a key target for type 2 diabetes (T2D) treatment. Because endocytic trafficking of agonist-bound receptors is one of the most important routes for regulation of receptor signaling, a better understanding of this process may facilitate the development of new T2D therapeutic strategies. Here, we screened 29 proteins with known functions in G protein–coupled receptor trafficking for their role in GLP-1R potentiation of insulin secretion in pancreatic β-cells. We identify five (clathrin, dynamin1, AP2, sorting nexins [SNX] SNX27, and SNX1) that increase and four (huntingtin-interacting protein 1 [HIP1], HIP14, GASP-1, and Nedd4) that decrease insulin secretion from murine insulinoma MIN6B1 cells in response to the GLP-1 analog exendin-4. The roles of HIP1 and the endosomal SNX1 and SNX27 were further characterized in mouse and human β-cell lines and human islets. While HIP1 was required for the coupling of cell surface GLP-1R activation with clathrin-dependent endocytosis, the SNXs were found to control the balance between GLP-1R plasma membrane recycling and lysosomal degradation and, in doing so, determine the overall β-cell incretin responses. We thus identify key modulators of GLP-1R trafficking and signaling that might provide novel targets to enhance insulin secretion in T2D.

The glucagon-like peptide-1 (GLP-1) receptor (GLP-1R) is a key type 2 diabetes therapeutic target (1). Upon agonist binding, GLP-1Rs signal through stimulatory G (Gs) proteins to raise intracellular cAMP levels and modulate insulin secretion from pancreatic β-cells.

As with other G protein–coupled receptors (GPCRs), GLP-1R signaling is tightly regulated through endocytic trafficking (2). Activated GLP-1Rs are rapidly internalized and recycled to the plasma membrane or distributed throughout endocytic compartments (3). Despite the pivotal role of trafficking in GPCR signaling, neither the molecular details nor the key factors responsible for GLP-1R endocytosis and postendocytic sorting have been thoroughly investigated.

Trafficking of the wider GPCR family has, however, been extensively characterized (4). After agonist binding and G protein recruitment, GPCRs undergo phosphorylation, β-arrestin recruitment, signal termination, and sorting into clathrin-coated pits (CCPs) for internalization (5). β-Arrestin recruitment also results in a second wave of signaling (6). Postendocytic GPCR sorting is critical for the spatiotemporal regulation of signaling (7) and involves numerous molecular players, including receptor posttranslational modifications (8), interactions with endosomal sorting complex required for transport (ESCRT) (9), PDZ domain–containing proteins (10), small guanosine-5′-triphosphatases (11), and membrane curvature–inducing sorting nexins (SNXs) (12). In addition, although endocytosis has long been associated with

[1]Section of Cell Biology and Functional Genomics and Pancreatic Islet Biology and Diabetes Consortium, Imperial College London, London, U.K.
[2]Section of Investigative Medicine, Imperial College London, London, U.K.
[3]New England Biolabs, Ipswich, MA
[4]Department of Surgery, University of Geneva, Geneva, Switzerland
[5]Diabetes Research Institute, San Raffaele Scientific Institute, Milan, Italy
[6]Vita-Salute San Raffaele University, Milan, Italy
[7]Department of Clinical and Experimental Medicine, Islet Cell Laboratory, University of Pisa, Pisa, Italy
[8]Nuffield Department of Surgical Sciences, University of Oxford, Oxford, U.K.
[9]Clinical Islet Laboratory and Clinical Islet Transplant Program, University of Alberta, Edmonton, Alberta, Canada

Corresponding author: Alejandra Tomas, a.tomas-catala@imperial.ac.uk.

Received 3 June 2017 and accepted 19 December 2017.

This article contains Supplementary Data online at http://diabetes.diabetesjournals.org/lookup/suppl/doi:10.2337/db17-0639/-/DC1.

signal attenuation, recent evidence indicates that signaling also occurs from endosomes (13).

In this study, we screened 29 factors known for their roles in GPCR trafficking to identify those that modulate incretin-stimulated insulin secretion (ISIS). Our approach identified nine factors as key regulators of incretin responses. We further characterized huntingtin-interacting protein 1 (HIP1), an endocytic factor involved in Huntington disease (HD) (14), and SNX1 and SNX27, endosomal factors associated with the multiprotein retromer complex (15), in GLP-1R signaling and β-cell function.

RESEARCH DESIGN AND METHODS

Cell/Islet Culture

Mouse MIN6B1 (derived from MIN6 [16]) cells were maintained as described (17). Stable MIN6B1–SNAP–GLP-1R and CHO-K1–SNAP–GLP-1R cells were generated by SNAP–GLP-1R transfection, G418 selection, and FACS after labeling with SNAP-Surface 488 probe (New England Biolabs). CHO-K1–GLP-1R–RLuc8 cells were generated by GLP-1R–RLuc8 transfection, G418 selection, and individual clone screening by luciferase assay. Human EndoC-βH1 cells were cultured as described (18).

Human islet studies were approved by the National Research Ethics Committee London (REC07/H0711/114). Islets isolated from normoglycemic donors with appropriate consent and ethical approval were cultured as described (19). See Supplementary Table 1 for donor details.

Confocal Microscopy

Cells were labeled with 1 μmol/L fluorescent SNAP-Surface probe (New England Biolabs) in HEPES-bicarbonate buffer (120 mmol/L NaCl, 4.8 mmol/L KCl, 24 mmol/L $NaHCO_3$, 0.5 mmol/L Na_2HPO_4, 5 mmol/L HEPES, 2.5 mmol/L $CaCl_2$, 1.2 mmol/L $MgCl_2$, 5% CO_2, pH 7.4) plus 3 mmol/L glucose and 1% BSA, stimulated with 100 nmol/L exendin-4 plus 11 mmol/L glucose, fixed, and imaged with a Zeiss LSM-780 inverted confocal microscope with a ×63/1.4 numerical aperture oil-immersion objective, and analyzed in ImageJ.

cAMP Assays

For static cAMP, cells were incubated in media with indicated glucose ± 100 nmol/L exendin-4/GLP-1 supplemented with isobutylmethylxanthine (IBMX) as indicated. Results were expressed versus baseline [cAMP] in IBMX. Note that exendin-4 cAMP responses were not affected by the glucose concentration (Supplementary Fig. 1). For exendin-4 dose-responses, CHO–SNAP–GLP-1R cells were stimulated without phosphodiesterase inhibitors, and a curve was fitted to a four-parameter logistic fit. For endosomal cAMP, cells were treated with 100 nmol/L exendin-4 for 15 min to allow internalization, followed by washing and 60 min in 10 μmol/L GLP-1R antagonist exendin (9-39) plus 10 μmol/L trafficking inhibitor monensin and the indicated IBMX concentration. Results were normalized to [cAMP] after 15 min exendin-4. cAMP was measured by cAMP Dynamic 2 homogeneous time-resolved fluorescence-based assay (Cisbio Bioassays) in a PHERAstar reader (BMG Labtech).

For cAMP Förster resonance energy transfer (FRET), cells were transfected with cAMP sensor Citrine/Cerulean-Epac2-camps (20) and imaged in HEPES-bicarbonate buffer plus 3 mmol/L glucose and 100 μmol/L IBMX before and after addition of 100 nmol/L exendin-4. Wavelengths were 440 nm (excitation), 470 nm (Cerulean emission), and 530 nm (Citrine emission). FRET is Cerulean/Citrine fluorescence normalized to baseline before exendin-4.

FACS Trafficking Assay

MIN6B1–SNAP–GLP-1R cells were labeled with 1 μmol/L cleavable O6-benzylguanine disulfide (BG-SS)-488 SNAP-Surface probe (a gift from New England Biolabs) and stimulated with 100 nmol/L exendin-4 before trafficking assays (21).

Briefly, to measure receptor internalization, cells were cooled at 4°C to arrest endocytosis after incubation at 37°C for the indicated times, or put at 4°C (t = 0 min), and treated with ice-cold alkaline Tris/NaCl/EDTA buffer (100 mmol/L NaCl, 50 mmol/L Tris-HCl, pH 8.6) ± 100 mmol/L sodium 2-mercaptoethanesulfonate (MesNa), a membrane-impermeable reducing agent, to strip surface-exposed label (+MesNa) or for total receptor (−MesNa). For recycling, cells were incubated with exendin-4 for 15 min, arrested at 4°C, MesNa-treated, incubated for 30 min with 10 μmol/L exendin(9-39) to prevent further internalization, and subjected to a second round of surface label removal.

Cells were processed by FACS using a BD LSR II flow cytometer (10,000 cells/sample) and analyzed with FlowJo: median fluorescence emission at 525 nm from living, single cells was measured, with highly auto-fluorescent cells excluded by dual fluorescence measurements at 525 and 585 nm.

The percentage of internalized receptor was calculated as follows:

$$\frac{\left(\frac{F_{+Me}(t_x)}{F_{-Me}(t_x)}\right) - \left(\frac{F_{+Me}(t_0)}{F_{-Me}(t_0)}\right)}{1 - \left(\frac{F_{+Me}(t_0)}{F_{-Me}(t_0)}\right)} \times 100$$

where F_{+Me} (t) and F_{-Me} (t) are median fluorescence ± MesNa at time t_x or t_0 (0 min). The percentage of recycled receptor was calculated by subtracting residual median fluorescence after the recycling protocol from that measured at t = 15 min and normalizing it to the percentage of internalized receptor at t = 15 min.

Electron Microscopy

MIN6B1–SNAP–GLP-1R cells cultured on Thermanox coverslips (Agar Scientific) were labeled with 2 μmol/L SNAP-Surface biotin (a gift from New England Biolabs) and 5 μg/mL NaN_3-free Alexa Fluor 488 Streptavidin, 10 nm colloidal gold (Molecular Probes) and stimulated with 100 nmol/L exendin-4. Conventional electron microscopy was performed as described (22). Ultrathin 70-nm sections were cut en face with a diamond knife (DiATOME) and

imaged on an FEI Tecnai G2 Spirit transmission electron microscope. Images were acquired in a charge-coupled device camera (Eagle), and gold particles were quantified in ImageJ.

Insulin Secretion Assays

Cells were preincubated at 37°C in a Krebs-HEPES-bicarbonate (KHB) buffer (140 mmol/L NaCl, 3.6 mmol/L KCl, 1.5 mmol/L $CaCl_2$, 0.5 mmol/L $MgSO_4$, 0.5 mmol/L NaH_2PO_4, 2 mmol/L $NaHCO_3$, 10 mmol/L HEPES, and 1% BSA [MIN6B1]; 460 mmol/L NaCl, 20 mmol/L KCl, 4 mmol/L $CaCl_2$, 4 mmol/L $MgCL_2$, 96 mmol/L $NaHCO_3$ and 0.2% BSA [EndoC-βH1]; 5% CO_2, pH 7.4) plus 3 mmol/L (MIN6B1) or 0.5 mmol/L (EndoC-βH1) glucose, then incubated 1 h at 37°C in KHB buffer plus 11 mmol/L (MIN6B1) or 15 mmol/L (EndoC-βH1) glucose ± 100 nmol/L exendin-4/GLP-1, and supernatants and cell extracts were recovered. Insulin was measured as described (23) and expressed as the insulin stimulation index (ISI) relative to 11 or 15 mmol/L glucose alone. Human islet assays were performed as described (19).

TUNEL Assays

MIN6B1 cells were incubated overnight with serum-free media plus 25 mmol/L glucose and 0.5 mmol/L palmitate/BSA ± 100 nmol/L exendin-4, processed with the In Situ Cell Death Detection Kit (Roche), and imaged, with ≥500 cells counted per experiment.

cDNA Transfections and RNA Interference

Transient cDNA/small interfering RNA (siRNA) transfections were performed with Lipofectamine 2000 (Life Technologies), for 48 and 72 h, respectively (see Supplementary Table 2 for a plasmid list). Mouse RNA interference (RNAi) sequences were ON-TARGETplus Nontargeting Control Pool and SMARTpools from a Cherry-pick RNAi Library (Dharmacon) (see Supplementary Table 3 for details). Hamster RNAi sequences were 5′-CATAATAACCAGAAGATGATT-3′ (SNX1) and 5′-GAACAAGACTGAAGAGGGATT-3′ (SNX27).

For the HIP1 lentiviral short hairpin RNA (shRNA), a control and five human HIP1 shRNA constructs (Dharmacon), based on target sequences from The RNAi Consortium (Supplementary Fig. 6*A*), were transfected onto HEK293T to assess knockdown efficiency. Two constructs displaying the highest knockdown were selected for lentiviral particle production. Intact human islets were infected at multiplicity of infection (MOI) 20 and cultured for 72 h before analysis.

Stable EndoC-βH1 SNX shRNA sublines were generated by infection with lentiviral particles expressing shRNA duplexes previously cloned into pLKO.3G. See Supplementary Fig. 11*A* for target sequence details.

Lentiviral Packaging

Lentiviruses were generated in HEK293T cells by cotransfection of shRNA with envelope and packaging vectors. Viral supernatants were harvested and purified by 20% sucrose gradient ultracentrifugation.

Cytosolic Ca^{2+} Imaging in Human Islets

Ca^{2+} imaging was performed as described (24). Islets loaded with 10 μmol/L Fluo-2 in HEPES-bicarbonate buffer plus 11 mmol/L glucose were imaged by sequential perifusion of 100 nmol/L exendin-4 (15 min) and 20 mmol/L KCl (4 min). Emitted signals (510–540 nm) were captured at 30 min^{-1} frame rates, and normalized by average baseline fluorescence.

Quantitative PCR

Quantitative real-time PCR (qRT-PCR) was performed using standard methodologies with SYBR Green primers designed using Primer Express.

Pull-Down Assays

MIN6B1–SNAP–GLP-1R cells were stimulated with 100 nmol/L exendin-4, cross-linked with 2 mmol/L 3,3′-dithiodipropionic acid di(*N*-hydroxysuccinimide ester) (Sigma-Aldrich), quenched with 20 mmol/L Tris-HCl (pH 7.5), and lysed in 20 mmol/L Tris, 150 mmol/L NaCl, 1 mmol/L EDTA, 1 mmol/L EGTA, 0.5% Triton X-100 plus cOmplete Mini EDTA-free protease inhibitor (Roche), and phosphatase inhibitor (Sigma-Aldrich) cocktails. Lysates were precleared with Protein G-Agarose beads (Roche) and incubated with SNAP-Capture Pull-Down Resin beads (New England Biolabs). Beads were washed five times, resuspended in urea sample buffer (100 mmol/L Tris-HCl [pH 6.8], 2.5% SDS, 4 mol/L urea, 50 mmol/L dithiothreitol, 0.05% bromophenol blue), and incubated for 10 min at 37°C before immunoblotting.

Western Immunoblotting

Lysates fractioned by SDS-PAGE under reducing conditions were immunoblotted using standard methodologies. Antibodies are listed in Supplementary Table 4.

Bioluminescence Resonance Energy Transfer Saturation Assay

CHO–GLP-1R–RLuc8 cells were transfected with increasing amounts of SNX27-green fluorescent protein (GFP), and bioluminescence resonance energy transfer (BRET) assays were performed as described (25). Briefly, 5 μmol/L coelenterazine *h* was added, and bioluminescence and fluorescence were recorded at 475 and 530 nm in a FlexStation 3 plate reader (Molecular Devices). Average BRET ratios were calculated as 530 nm–to–475 nm signals, and net BRET values were obtained by subtracting the basal BRET ratio of GLP-1R–Rluc8 alone.

Statistical Analyses

GraphPad Prism 7.0 software was used for data analyses. ANOVA or two-tailed *t* tests were performed throughout. Paired analyses were used in experiments with matched designs.

RESULTS

RNAi Screen of GLP-1R Trafficking Regulators

We selected 29 factors with known effects in GPCR trafficking (Supplementary Table 5), including regulators

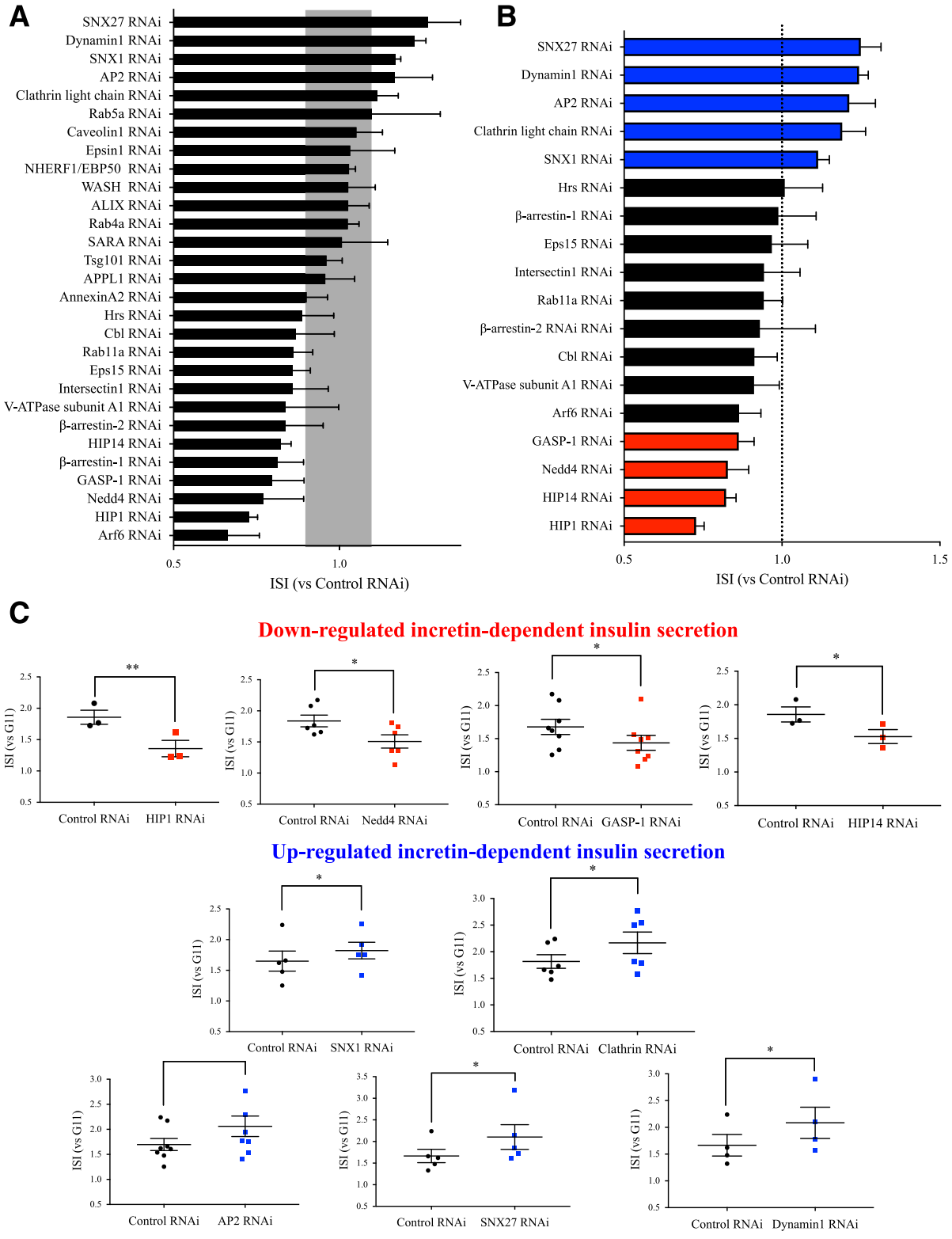

Figure 1—RNAi screen of GPCR endocytic trafficking regulators in MIN6B1–SNAP–GLP-1R cells. *A*: First round screen of ISIS after RNAi silencing of 29 candidate trafficking regulators. Results are expressed as mean ± SEM of ISI for each candidate of exendin-4 in 11 mmol/L glucose (G11) relative to G11 alone and normalized to control RNAi for each candidate ($n = 3$). The gray bar represents 10% cutoff effect on ISI vs. control RNAi. *B*: Further analysis of ISIS after knockdown of 18 candidates selected from the initial screen. Results are expressed as above ($n = 3$–8). Factors with significant upregulated secretion after RNAi are depicted in blue, and those with significant RNAi-induced downregulation of secretion are in red. *C*: Individual results for each of the factors from *B* presenting a significant ISIS effect after knockdown, relative to paired control RNAi experiments. Data are expressed as mean ± SEM of exendin-4 plus G11 ISI relative to G11 alone ($n = 3$–8). Individual data points are shown. $^*P < 0.05$ and $^{**}P < 0.01$, two-tailed paired *t* tests.

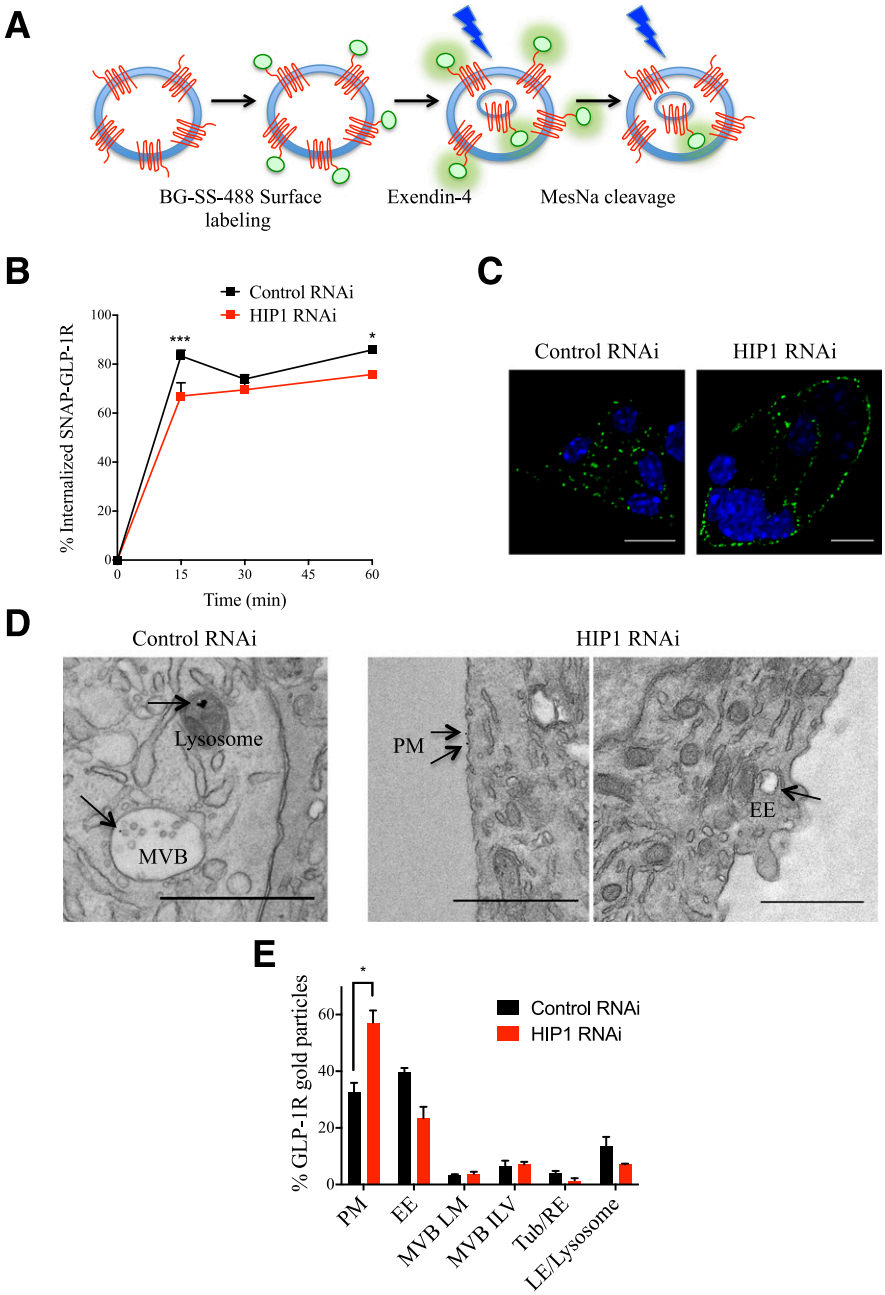

Figure 2—Role of HIP1 in GLP-1R trafficking in MIN6B1–SNAP–GLP-1R cells. *A*: Schematic shows the protocol for FACS analysis of SNAP–GLP-1R trafficking. *B*: Percentage of SNAP–GLP-1R internalization after treatment with 100 nmol/L exendin-4 in control vs. HIP1 RNAi-treated MIN6B1–SNAP–GLP-1R cells. Data are expressed as mean ± SEM ($n = 3$). *$P < 0.05$ and ***$P < 0.001$, two-way randomized block ANOVA with the Sidak test. *C*: Confocal microscopy results show SNAP–Surface-488–labeled SNAP–GLP-1R (green) in control vs. HIP1 RNAi-treated MIN6B1–SNAP–GLP-1R cells after 15-min stimulation with 100 nmol/L exendin-4. Nuclei (DAPI), blue. Size bars, 10 μm. *D*: Electron microscopy localization of SNAP–GLP-1R (gold particles, arrows) in control vs. HIP1 siRNA-transfected MIN6B1–SNAP–GLP-1R cells treated as above. Size bars, 1 μm. After 15-min stimulation with exendin-4, the receptor is present in the multivesicular body (MVB)/late endosome (LE)/lysosomal compartment in control RNAi but is still primarily localized to plasma membrane (PM)/early endosomes (EEs) after HIP1 RNAi. *E*: Gold-particle quantification of percentage of SNAP–GLP-1R in each subcellular organelle. Data are expressed as mean ± SEM ($n = 2$). *$P < 0.05$, two-tailed paired *t* test. LM, limiting membrane; ILV, intraluminal vesicles; Tub/RE, tubular/recycling endosomes.

of posttranslational modifications (HIP14, Cbl, Nedd4); β-arrestins; clathrin-dependent (Intersectin1, HIP1, Epsin1, Eps15, AP2, clathrin, dynamin1) and clathrin-independent (Arf6, caveolin1) endocytosis modulators; early endosome biogenesis (Rab5a, AnnexinA2) and signaling (APPL1, SARA) factors; PDZ domain or retromer-associated factors (WASH, NHERF1, SNX27, SNX1); ESCRT-associated factors (Hrs, Tsg101, ALIX); and recycling (Rab11a, Rab4a), late endosome (GASP-1), and lysosomal (v-ATPase subunit) components. Gene expression was confirmed in MIN6B1

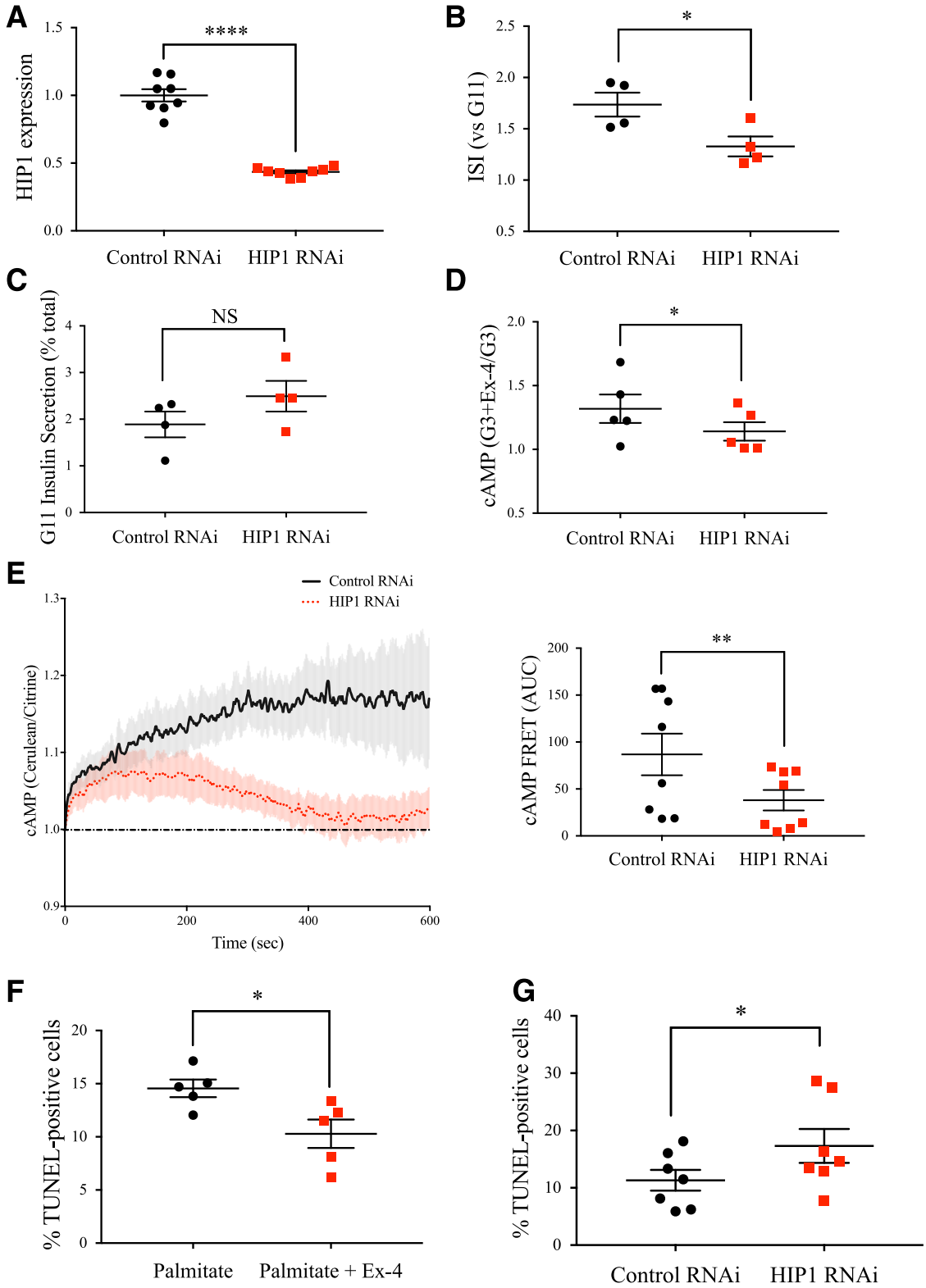

Figure 3—Effect of HIP1 RNAi on incretin responses from MIN6B1 cells. *A*: Knockdown efficiency determined by qRT-PCR in MIN6B1 cells at 48 h relative to control RNAi. Data are expressed as mean ± SEM (n = 8). Individual data points are shown. ****$P < 0.0001$, two-tailed t test. *B*: Exendin-4–stimulated insulin secretion of control vs. HIP1 RNAi-treated MIN6B1 cells. Data are expressed as mean ± SEM of exendin-4 plus 11 mmol/L glucose (G11) ISI relative to G11 alone (n = 4). Individual data points are shown. *$P < 0.05$, two-tailed paired t test. *C*: Glucose-stimulated insulin secretion of control vs. HIP1 RNAi-treated MIN6B1 cells from *B*. Data are expressed as mean ± SEM of insulin secreted at G11 as percentage of total insulin (n = 4). Individual data points are shown. NS, two-tailed paired t test. *D*: Incretin-induced cAMP after 1-h treatment with 3 mmol/L glucose (G3) + 100 nmol/L exendin-4 (Ex4) and 100 μmol/L IBMX in control vs. HIP1 RNAi-treated MIN6B1 cells. Data are expressed as mean ± SEM of exendin-4 + 100 μmol/L IBMX relative to 100 μmol/L IBMX alone (n = 5). Individual data points are shown. *$P < 0.05$, two-tailed paired t test. *E*: cAMP FRET time-course response (left) and area under the curve (AUC, right) for 10-min stimulation with

cells with the exception of caveolin1, which was below detection levels (Supplementary Fig. 2*A*).

Candidates were silenced by RNAi (Supplementary Fig. 2*B*) in a MIN6B1 subline stably expressing SNAP-tagged human GLP-1R, MIN6B1–SNAP–GLP-1R, where follow-up trafficking studies could be performed. Insulin secretion in response to the stable GLP-1 analog exendin-4 was measured (Fig. 1). Factors with <10% effect were discarded in a first round of screening (Fig. 1*A*). From the remaining factors, we identified five (SNX27, dynamin1, AP2, clathrin, and SNX1) that increased and four (HIP1, Nedd4, HIP14, and GASP-1) that decreased ISIS upon gene silencing (Fig. 1*B* and *C*). We selected the factors with the strongest effect, that is, HIP1 and the SNX27 (together with its retromer partner, SNX1), for further analysis.

HIP1 Regulates GLP-1R Trafficking and Signaling

We first determined the effect of HIP1 silencing on GLP-1R trafficking with a FACS trafficking assay in MIN6B1–SNAP–GLP-1R cells (see RESEARCH DESIGN AND METHODS and Fig. 2*A* for details). We measured a small but significant reduction in exendin-4–induced SNAP–GLP-1R internalization in HIP1 versus control RNAi (Fig. 2*B*), without effect on recycling (Supplementary Fig. 3). This internalization delay was confirmed by confocal (Fig. 2*C*) and electron microscopy (Fig. 2*D*, quantified in Fig. 2*E*).

The MIN6B1–SNAP–GLP-1R subline allows correlation between secretion and trafficking but overexpresses the GLP-1R compared with parental MIN6B1 cells (Supplementary Fig. 4). Experiments were therefore repeated in the more physiological MIN6B1 cells and primary human islets. HIP1 RNAi (Fig. 3*A*) caused a significant decrease in insulin secretion in MIN6B1 in response to exendin-4 (Fig. 3*B*) and to the natural agonist GLP-1 (Supplementary Fig. 5), whereas glucose-stimulated insulin secretion (GSIS) was unaffected (Fig. 3*C*). Reduced GLP-1R signaling was confirmed by static and dynamic (FRET) cAMP experiments (Fig. 3*D* and *E*). There was also a significant reduction in the protection against glucolipotoxicity-induced apoptosis by exendin-4 after HIP1 knockdown (Fig. 3*F* and *G*).

For human islets, we selected two HIP1 shRNA constructs with high knockdown efficiency (Supplementary Fig. 6*A* and *B*) to produce lentiviral particles. Efficient silencing was confirmed in human EndoC-βH1 β-cells plus dispersed (Supplementary Fig. 6*C* and *D*) and intact human islets (Fig. 4*A* and *B*), where functional studies were performed. HIP1 silencing significantly decreased ISIS (Fig. 4*C*) without affecting GSIS (Supplementary Fig. 6*E*). Exendin-4–induced cytosolic Ca^{2+} rises were also decreased (Fig. 4*D* and *E*), whereas Ca^{2+} response to KCl was unaffected (Fig. 4*F*).

We next determined the effect of HIP1 knockdown on β-arrestin recruitment (Fig. 5*A*). Recruitment of β-arrestins to SNAP–GLP-1R, not detected under vehicle conditions (Supplementary Fig. 7), was clearly present after 5 min exendin-4 in control, but was highly reduced in HIP1 RNAi-treated MIN6B1–SNAP–GLP-1R cells.

Then we performed a pull-down assay to isolate factors interacting with SNAP–GLP-1R after HIP1 RNAi (Fig. 5*B*). We isolated β-arrestin-1–monomeric yellow fluorescent protein (mYFP) and β-arrestin-2–GFP in complex with SNAP–GLP-1R after 5 min exendin-4 in control cells, confirming that GLP-1R recruits both arrestin isoforms; however, this association was impaired after HIP1 knockdown. In addition, we detected binding of GLP-1R to Gs α subunit (GαS)-YFP in control but not in HIP1 RNAi-treated cells, as well as reduced binding to tyrosine kinase Src, normally recruited to agonist-bound GLP-1R via β-arrestin-1 (26).

Finally, we performed a rescue experiment by expressing human full-length or mutant HIP1 deleted for the clathrin-binding domain in control or HIP1 RNAi-treated MIN6B1 cells (Fig. 5*C*). As expected, full-length but not clathrin-binding deficient HIP1 restored the capacity of SNAP–GLP-1R to internalize with exendin-4 (Fig. 5*D*). However, both forms of HIP1 rescued ISIS from HIP1-depleted cells to a similar extent (Fig. 5*E*), despite reduced levels of expression of clathrin-binding domain-deleted versus full-length HIP1 (Fig. 5*C*).

SNX1 and SNX27 Regulate GLP-1R Recycling and Insulin Secretion

In the second part of the study, we analyzed the roles of SNX1 and SNX27 in GLP-1R trafficking and signaling. We noticed a high degree of colocalization (Fig. 6*A*) and protein interaction (Fig. 6*B*) between SNAP–GLP-1R and GFP-tagged SNX1 and SNX27, which was greater for SNX27-GFP. We confirmed the interaction between GLP-1R–RLuc8 and SNX27-GFP by BRET (Fig. 6*C*). This interaction was still present for mutant SNX27 either bearing a point mutation in the NPxY-binding domain or lacking the PDZ domain (Supplementary Fig. 8).

We next analyzed GLP-1R trafficking by FACS after SNX silencing. Surprisingly, although downregulation of both SNXs increased ISIS (Fig. 1) and cAMP (Supplementary Fig. 9) in MIN6B1–SNAP–GLP-1R cells, SNX1 knockdown increased while SNX27 knockdown decreased SNAP-GLP-1R plasma membrane recycling (Fig. 7*A* and *B*). No effects on

100 nmol/L exendin-4 plus 100 μmol/L IBMX in control vs. HIP1 RNAi-treated MIN6B1 cells. Data are normalized to baseline (recorded for 5 min before exendin-4 addition) and expressed as mean ± SEM (n = 8 cells from four independent experiments). Individual data points are shown. $^{**}P < 0.01$, two-tailed paired t test. *F*: Percentage of TUNEL-positive MIN6B1 cells after overnight incubation with 0.5 mmol/L palmitate/BSA in the presence or absence of 100 nmol/L exendin-4. Data are mean ± SEM (n = 5). Individual data points are shown. $^{*}P < 0.05$, two-tailed paired t test. *G*: Percentage of TUNEL-positive MIN6B1 cells transfected with control vs. HIP1 siRNA after overnight incubation with 0.5 mmol/L palmitate/BSA + 100 nmol/L exendin-4. TUNEL staining in untreated (no palmitate or exendin-4 added) cells was typically <5%. Data are mean ± SEM (n = 7). Individual data points are shown. $^{*}P < 0.05$, two-tailed paired t test.

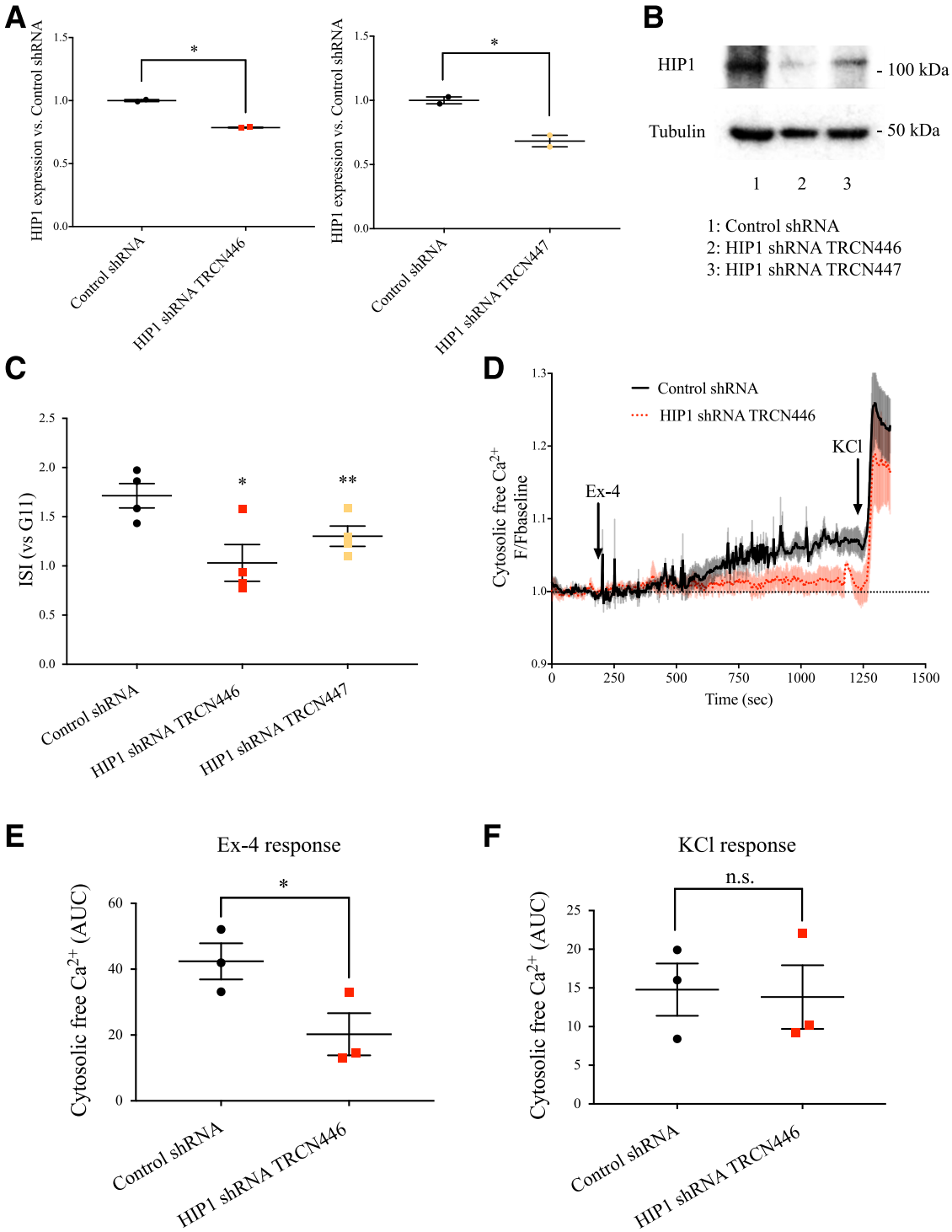

Figure 4—Effect of HIP1 knockdown on incretin responses from human donor islets. *A*: Knockdown efficiency determined by qRT-PCR at 72 h from intact human islets infected with human HIP1 shRNA lentiviruses, relative to control shRNA infection (n = 2); HIP1 shRNA TRCN0000033446, TRCN446; HIP1 shRNA TRCN0000033447, TRCN447. Individual data points are shown. *$P < 0.05$ vs. control shRNA, two-tailed paired t test. *B*: Western blot analysis of HIP1 levels (top) from lysates of intact human islets infected with lentiviruses for control shRNA or HIP1 shRNA TRCN446 or TRCN447 for 72 h, with tubulin as the loading control (bottom). *C*: ISIS from human donor islets infected with control vs. HIP1 shRNA lentiviruses TRCN446 or TRCN447. Data are expressed as mean ± SEM of exendin-4 + 11 mmol/L glucose (G11) ISI relative to G11 alone (n = 4). Individual data points are shown. *$P < 0.05$ and **$P < 0.01$ vs. control shRNA, one-way randomized block ANOVA with the Dunnett test. *D*: Ca^{2+} time-course responses from Fluo-2–loaded human islets infected with control vs. HIP1 shRNA lentivirus TRCN446 after sequential stimulations with exendin-4 (Ex-4) (100 nmol/L) for 15 min and KCl (20 mmol/L) for 4 min. Area under the curve (AUC) corresponding to exendin-4 (*E*) or KCl (*F*) responses from *D*, calculated from data normalized to baseline. Data are expressed as mean ± SEM (n = 3; 9–13 islets imaged per experiment). Individual data points are shown. *$P < 0.05$, two-tailed paired t test.

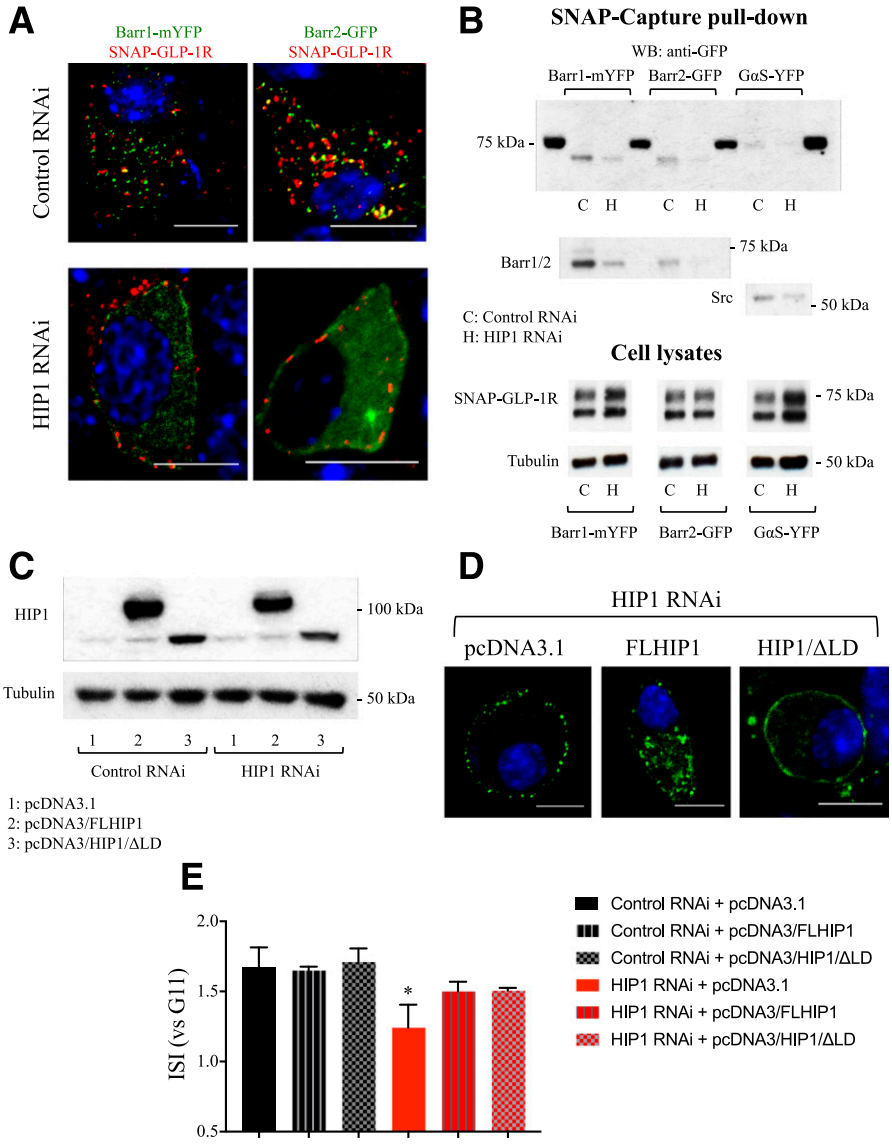

Figure 5—Regulation of GLP-1R activation by HIP1. *A*: Confocal microscopy shows colocalization of SNAP–GLP-1R and β-arrestin-1–mYFP (Barr1-mYFP) or β-arrestin-2–GFP (Barr2-GFP) in control (top) or HIP1 RNAi-treated MIN6B1–SNAP–GLP-1R cells (bottom) after 5 min of 100 nmol/L exendin-4 exposure. β-Arrestin-1–mYFP or β-arrestin-2–GFP (green); SNAP–GLP-1R (labeled with SNAP-Surface-549), red; nuclei (DAPI), blue. Size bars, 10 μm. *B*: SNAP-Capture pull-down of SNAP–GLP-1R with β-arrestin-1–mYFP, β-arrestin-2–GFP, or GαS-YFP from lysates of control vs. HIP1 RNAi-treated MIN6B1–SNAP–GLP-1R cells after 5-min exposure to 100 nmol/L exendin-4 (top). Pulled-down proteins analyzed by Western blot (WB) for GFP/mYFP, β-arrestin-1/-2, and Src. Original lysates were analyzed by Western blot for SNAP to assess levels of SNAP–GLP-1R and tubulin as the loading control (bottom). *C*: Western blot analysis of human HIP1 levels (top) in lysates from control or mouse HIP1-RNAi-treated MIN6B1 cells retransfected with empty pcDNA3.1 or plasmids expressing human full-length HIP1 (pcDNA3/FLHIP1) or mutant HIP1 with deleted clathrin-binding domain (pcDNA3/HIP1/ΔLD [LMD and DPF motifs]), with tubulin as the loading control (bottom). Note that cells were retransfected with DNA plasmids 24 h after initial RNAi transfection and further incubated for 48 h before experiments and that the HIP1 antibody used in this study primarily detects human rather than mouse HIP1. *D*: Confocal microscopy results show SNAP–Surface-488–labeled SNAP–GLP-1R (green) in HIP1 RNAi-treated MIN6B1–SNAP–GLP-1R cells retransfected with plasmids as in *C* after 15-min stimulation with 100 nmol/L exendin-4. Nuclei (DAPI), blue. Size bars, 10 μm. *E*: ISIS of control vs. HIP1 RNAi-treated MIN6B1 cells retransfected with each of the three plasmids shown in *C* and *D*. Data are expressed as mean ± SEM of exendin-4 + 11 mmol/L glucose (G11) ISI relative to G11 alone ($n = 3$). *$P < 0.05$ vs. control shRNA + pcDNA3.1, one-way randomized block ANOVA with the Dunnett test.

internalization were detectable. It has been reported that SNX27 silencing, while reducing receptor recycling, can increase signaling from endocytic compartments (27). To test this hypothesis, we measured exendin-4–induced cAMP production specifically from internalized receptors (Fig. 7*C*). This revealed a significant increase after SNX27, but not SNX1, knockdown, suggesting that cAMP increases after SNX1 and SNX27 silencing have different subcellular origins. We also performed a degradation assay to measure SNAP–GLP-1R levels before and after exendin-4 stimulation but did not detect any significant effect of either SNX RNAi (Fig. 7*D*). Thus, modest reductions in SNX expression (Supplementary Fig. 2*B*) primarily affect GLP-1R recycling, without affecting basal or exendin-4–induced lysosomal degradation.

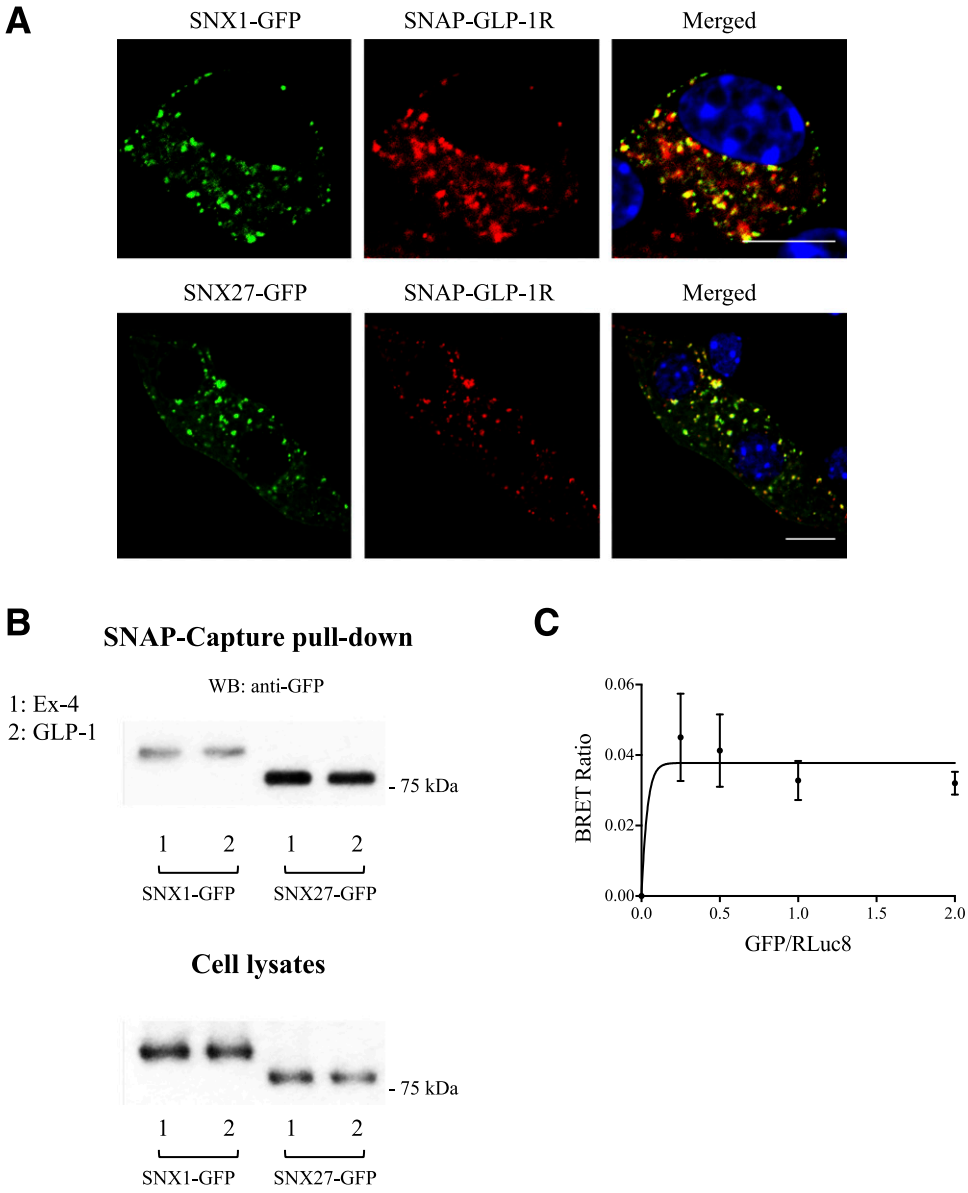

Figure 6—Association of SNAP–GLP-1R with SNX1-GFP and SNX27-GFP. *A*: Confocal microscopy shows colocalization of SNAP–GLP-1R and SNX1-GFP or SNX27-GFP in MIN6B1–SNAP–GLP-1R cells after 15-min treatment with 100 nmol/L exendin-4. SNX1-GFP or SNX27-GFP (green); SNAP–GLP-1R (labeled with SNAP–Surface-549), red; nuclei (DAPI), blue. Size bars, 10 μm. *B*: SNAP-Capture pull-down of SNAP–GLP-1R with SNX1-GFP or SNX27-GFP from MIN6B1–SNAP–GLP-1R cell lysates after 15-min exposure to 100 nmol/L exendin-4 (Ex-4) or GLP-1. Pulled-down proteins analyzed by Western blot (WB) for GFP. Original lysates were immunoblotted to assess levels of expression of GFP-tagged SNX constructs. *C*: Saturation curves from BRET ratios with the indicated amounts of SNX27-GFP plasmid DNA in CHO–GLP-1R–RLuc8 cells after 15-min treatment with 100 nmol/L exendin-4. Data are mean ± SEM (n = 3).

We next confirmed our findings in parental MIN6B1 cells where, after mild (~40%) SNX1 or SNX27 downregulation (Fig. 7*E*), ISIS was again significantly increased (Fig. 7*F*).

SNX27 depletion has been linked to reductions in basal receptor levels (28,29). To investigate whether a higher degree of knockdown might also cause similar effects for GLP-1R, we performed SNX knockdown experiments using a subline of readily transfectable CHO-K1 cells stably expressing SNAP–GLP-1R (CHO–SNAP–GLP-1R) (Supplementary Fig. 10), where SNX knockdown efficiency was ~70% (Fig. 8*A*). Exendin-4 cAMP dose-response curves showed that although the maximal response was increased after SNX1 downregulation, this was now reduced after SNX27 knockdown (Fig. 8*B*, left). We also overexpressed each SNX fused to GFP and compared cAMP responses to exendin-4 with those for GFP alone (Fig. 8*B*, right). SNX1-GFP reduced, whereas SNX27-GFP increased, maximal cAMP increases, effectively reversing the silencing results. Under these knockdown conditions, SNX27 RNAi-treated cells failed to sustain endosomal cAMP increases (Fig. 8*C*) and displayed reduced basal levels of SNAP–GLP-1R as well as increased exendin-4–induced receptor degradation (Fig. 8*D*).

Finally, we confirmed these results in stable SNX shRNA-expressing EndoC-βH1 human β-cells with silencing

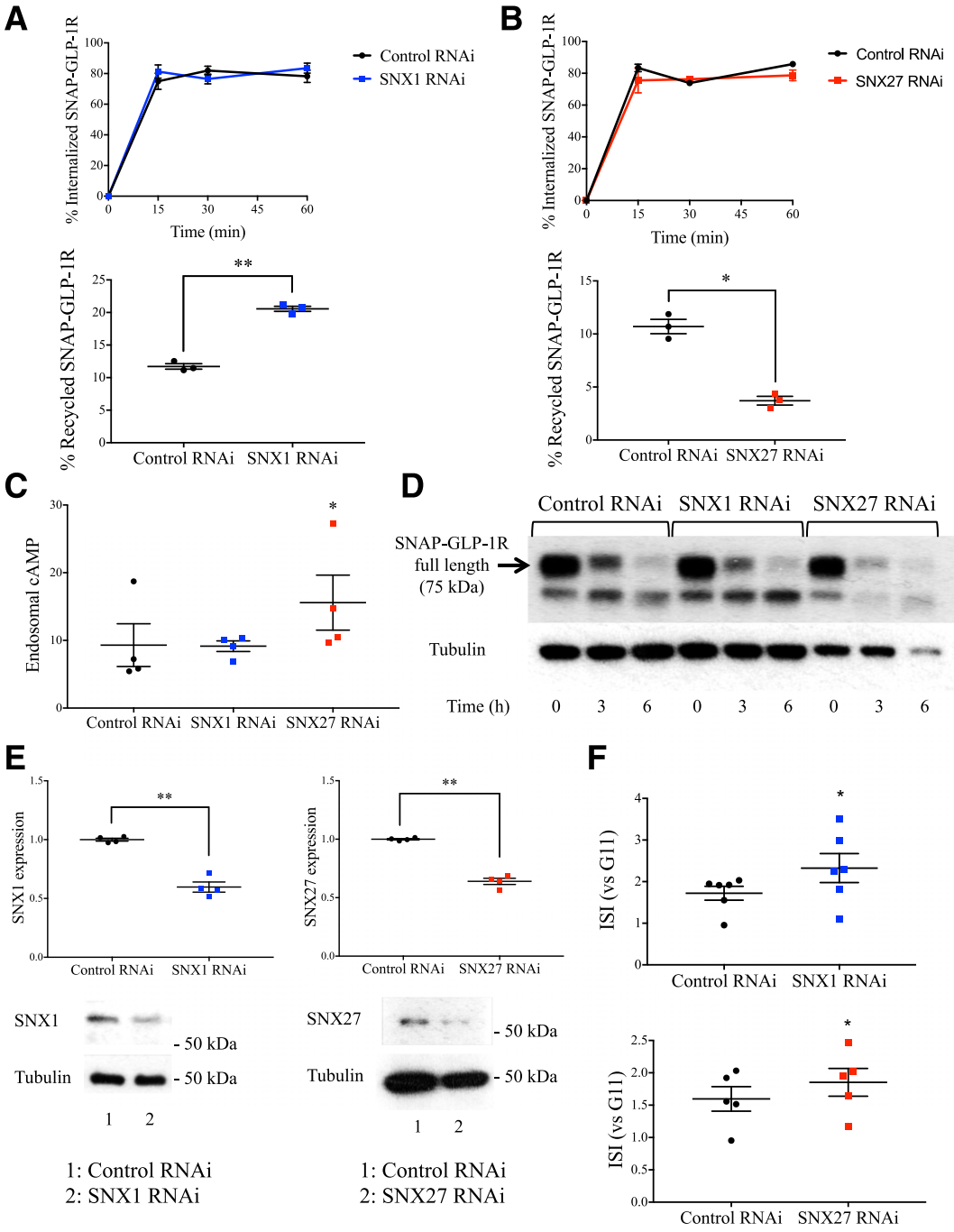

Figure 7—Effect of SNX1 and SNX27 RNAi on GLP-1R trafficking and incretin responses from MIN6B1 cells. *A* and *B*: Percentage of SNAP–GLP-1R internalization (top) and recycling (bottom) after treatment with 100 nmol/L exendin-4 in control vs. SNX1 (*A*) or SNX27 (*B*) RNAi-treated MIN6B1–SNAP–GLP-1R cells. Data are expressed as mean ± SEM (n = 3). Individual data points are shown for recycling. *$P < 0.05$ and **$P < 0.01$, two-tailed paired t test. *C*: Incretin-induced cAMP specifically from GLP-1Rs internalized into endosomes, measured after 15-min treatment with 100 nmol/L exendin-4, followed by washout and 60-min incubation in 10 μmol/L exendin(9-39) plus 10 μmol/L trafficking inhibitor monensin and 500 μmol/L IBMX in control vs. SNX1 or SNX27 RNAi-treated MIN6B1–SNAP–GLP-1R cells. Data are expressed as mean ± SEM of results normalized to 15 min of exendin-4 (n = 4). Individual data points are shown. *$P < 0.05$, one-way randomized block ANOVA with the Dunnett test. *D*: Western blot analysis of SNAP–GLP-1R levels in control vs. SNX1 or SNX27 RNAi-treated MIN6B1–SNAP–GLP-1R cells before and after exposure to 100 nmol/L exendin-4 for the indicated times. Cells were pretreated for 1 h with 100 μg/mL cycloheximide before exendin-4 treatment. Lysates were analyzed by Western blot with anti-SNAP to assess levels of SNAP–GLP-1R (top) and tubulin as the loading control (bottom). A degradation band corresponding to deletion of the receptor COOH-terminal domain is typically detected under all conditions analyzed. *E*: SNX1 and SNX27 knockdown efficiencies determined by qRT-PCR (at 48 h, top) and Western blotting (at 72 h, bottom) in MIN6B1 cells relative to control RNAi. Data are expressed as mean ± SEM (n = 4). Individual data points are shown. **$P < 0.01$, two-tailed t test. *F*: ISIS of control vs. SNX1 (top) or SNX27 (bottom) RNAi-treated MIN6B1 cells. Data are expressed as mean ± SEM of exendin-4 + 11 mmol/L glucose (G11) ISI relative to G11 alone (n = 6 for SNX1 RNAi and n = 5 for SNX27 RNAi). Individual data points are shown. *$P < 0.05$, two-tailed paired t test.

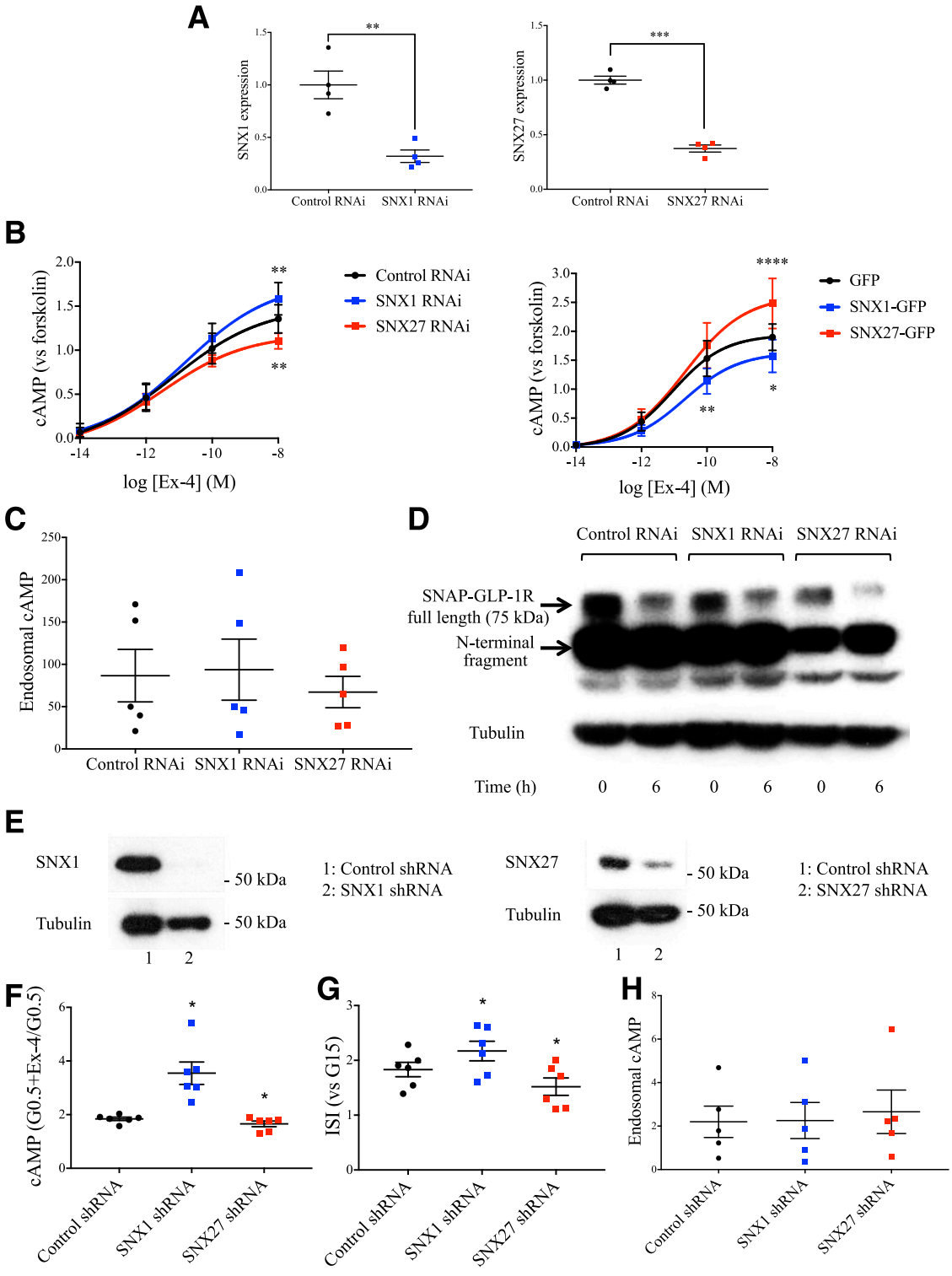

Figure 8—Effect of SNX1 and SNX27 RNAi on incretin responses from CHO–SNAP–GLP-1R and EndoC-βH1 cells. *A*: SNX1 (left) and SNX27 (right) knockdown efficiencies in CHO-SNAP–GLP–1R cells determined by qRT-PCR at 48 h, relative to control RNAi. Data are expressed as mean ± SEM (n = 4). Individual data points are shown. $^{**}P < 0.01$ and $^{***}P < 0.001$ by two-tailed t test. *B*: cAMP responses from CHO–SNAP–GLP-1R cells treated with control vs. SNX1 or SNX27 RNAi (left) or expressing GFP vs. SNX1-GFP or SNX27-GFP (right), after 15-min exendin-4 (Ex-4) incubation. Results are normalized to forskolin responses, four-parameter logistic fit of mean data ± SEM (n = 4). $^{*}P < 0.05$, $^{**}P < 0.01$, and $^{****}P < 0.0001$ vs. control RNAi or empty GFP by two-way randomized block ANOVA with the Dunnett test. *C*: Incretin-induced cAMP specifically from GLP-1Rs internalized into endosomes, measured after 15-min treatment with 100 nmol/L exendin-4, followed by washout and 60-min incubation in 10 μmol/L exendin(9-39) plus 10 μmol/L trafficking inhibitor monensin in control vs. SNX1 or SNX27 RNAi-treated CHO–SNAP–GLP-1R cells. Data are expressed as mean ± SEM of results normalized to 15 min of exendin-4 (n = 5). Individual data points are shown; NS by one-way randomized block ANOVA with the Dunnett test. *D*: Western blot analysis of SNAP–GLP-1R levels in control vs. SNX1 or SNX27 RNAi-treated CHO–SNAP–GLP-1R cells before and after exposure to 100 nmol/L exendin-4 for 6 h. Lysates were analyzed by Western blot with

efficiencies of ~80% (Fig. 8*E* and Supplementary Fig. 11*A* and *B*). Exendin-4–induced cAMP and insulin responses were again increased after SNX1 silencing, and a small but significant decrease was measured for SNX27 knockdown (Fig. 8*F* and *G*, also shown for GLP-1 responses in Supplementary Fig. 11*C* and *D*). Endosomal cAMP was again not increased in SNX27 versus control or SNX1 downregulated EndoC-βH1 cells (Fig. 8*H*).

DISCUSSION

Trafficking factors can radically alter GPCR signaling outputs (4). The GLP-1R has long been recognized as an important β-cell pharmacological regulator, and therefore, understanding the mechanisms that determine its downstream signaling is of considerable importance.

Here, we deployed a screen to identify trafficking factors with promising effects on insulin secretion downstream of GLP-1R. Importantly, the degree of screen silencing was quite modest (20–70%) (Supplementary Fig. 2*B*), further emphasizing the likely significance of the factors identified. Among factors that increased secretion after knockdown, we identified three—dynamin1, AP2, and clathrin—involved in CCP formation (30). This, together with the undetectable caveolin1 expression level in MIN6B1 cells and the reported interaction between GLP-1R and AP2 (31), suggests that the main route of GLP-1R internalization is clathrin-dependent.

A recent report (32) showed that nearly complete abrogation of receptor internalization with dominant negative dynamin1 leads to reduced GLP-1R signaling. The apparent discrepancy between this and our results may be related to the modest knockdown level achieved here for dynamin1. We hypothesize that a modest reduction in receptor internalization would preserve endosomal while allowing increased cell surface receptor signaling, resulting in overall signaling increases. In contrast, nearly complete inhibition of internalization might have detrimental effects due to complete abrogation of endosomal signaling and unmitigated β-arrestin–dependent cell surface receptor desensitization.

Silencing of individual β-arrestins had no significant effect on ISIS in our screen. This is in agreement with a recent report (33) showing normal GLP-1–induced insulin secretion in β-arrestin-2 knockout mice and might reflect some degree of redundancy between β-arrestin isoforms, although we note that β-arrestin-2 is >10-fold more expressed in MIN6B1 than β-arrestin-1 (Supplementary Fig. 2*A*). Alternatively, there may be compensation between increased plasma membrane but reduced β-arrestin–dependent or endosomal signaling. Among factors that reduced ISIS after knockdown, we found some involved in posttranslational modifications, such as the palmitoyl transferase HIP14 (34), or the ubiquitin ligase Nedd4 (35), as well as the late endosomal signaling factor GASP-1 (36).

Silencing of HIP1, an endocytic factor involved in clathrin-dependent receptor internalization (37), gave the strongest effect by decreasing ISIS, in contrast to other CCP components. This correlates with previous reports linking HIP1 with enhanced receptor activity and increased signaling (38). Loss of HIP1 also led to reduced exendin-4–induced SNAP–GLP-1R internalization and cAMP and cytosolic Ca^{2+} responses. Biochemical and structural studies have led to a "two-step" model of class B1 GPCR activation where, after agonist binding to free receptor, this "collides" with free G proteins (39), initiating the G protein signaling cascade. Our pull-down assays suggest that in the absence of HIP1, GLP-1R displays reduced G protein coupling, providing a mechanistic explanation for the observed reductions in receptor signaling and insulin secretion. As a result, there is impaired recruitment of β-arrestins and downstream factors such as Src.

Our rescue experiment not only confirms the importance of HIP1 but also unveils a role in coupling of GLP-1R activation with clathrin-dependent endocytosis. The HIP1 role in internalization appears not to be required for cell surface receptor signaling, because even with impaired internalization, HIP1 mutants unable to bind to clathrin rescued ISIS to the same extent as full-length HIP1 in HIP1-depleted cells. Notably, this was achieved despite reduced expression of mutant versus full-length HIP1, indicating that, in agreement with results obtained here for other CCP factors, reduced GLP-1R internalization when HIP1 is otherwise functional for receptor activation increases ISIS.

HIP1 interacts with the protein huntingtin in neurons, which, in its mutated form in the neurodegenerative syndrome HD, cannot associate with HIP1. Of interest is that patients with HD also present with impaired glucose handling, at least partially due to β-cell dysfunction (14). This dysfunction, and the general neurodegeneration, is alleviated by treatment with GLP-1R agonists, including exendin-4 (40). Although the effects of mutated huntingtin are complex and pleiotropic, it is possible that part of the glucose dysfunction is linked to deregulation of GLP-1R

anti-SNAP antibody to assess levels of SNAP–GLP-1R (top) and with tubulin as loading control (bottom). A degradation band corresponding to deletion of the receptor COOH-terminal domain is typically detected under all conditions analyzed. *E*: SNX1 (left) and SNX27 (right) knockdown efficiencies in control vs. SNX1 or SNX27 EndoC-βH1 shRNA sublines determined by Western blotting, with tubulin as loading control (bottom). *F*: Exendin-4–induced cAMP after 15-min treatment with 0.5 mmol/L glucose (G0.5) + 100 nmol/L exendin-4 and 500 μmol/L IBMX in control vs. SNX1 or SNX27 shRNA EndoC-βH1 sublines. Data are expressed as mean ± SEM of exendin-4 + 500 μmol/L IBMX relative to 500 μmol/L IBMX alone (n = 6). Individual data points are shown. *$P < 0.05$, one-way randomized block ANOVA with the Dunnett test. *G*: Exendin-4–stimulated insulin secretion of control vs. SNX1 or SNX27 shRNA EndoC-βH1 sublines. Data are expressed as mean ± SEM of exendin-4 + 15 mmol/L glucose (G15) ISI relative to G15 alone (n = 6). Individual data points are shown. *$P < 0.05$, one-way randomized block ANOVA with the Dunnett test. *H*: Incretin-induced cAMP specifically from GLP-1Rs internalized into endosomes, measured as in *C* but in control vs. SNX1 or SNX27 shRNA EndoC-βH1 sublines. Data are expressed as mean ± SEM of results normalized to 15-min exendin-4 (n = 5). Individual data points are shown; NS by one-way randomized block ANOVA with the Dunnett test.

signaling and hence directly ameliorated by pharmacological GLP-1R activation.

In addition, knockdown of the two SNXs in our screen, SNX27 and SNX1, led to increased exendin-4–induced cAMP and insulin secretion in MIN6B1–SNAP–GLP-1R cells. SNX1 interacts in vitro with the COOH-terminal domain of GLP-1R (41), and we demonstrate here this interaction in β-cells. SNX1 plays an important role in GPCR sorting toward degradation (42), but it has also been implicated in GPCR recycling modulation without affecting lysosomal turnover (43). Our findings are consistent with a role for SNX1 on restricting the rate of GLP-1R recycling without affecting overall degradation, leading to consistent increases on GLP-1R signaling and ISIS after its downregulation.

SNX27 is conversely involved in membrane tubulation and receptor sorting from early to recycling endosomes (44). Here we have found for the first time that GLP-1R strongly associates and interacts with SNX27 in β-cells. This is somewhat surprising because most associations of GPCRs with SNX27 are mediated by interactions between the SNX27 PDZ domain and PDZ-binding motifs at the receptor COOH-terminal domain (45). The GLP-1R does not contain a canonical PDZ-binding motif and, consequently, binds to SNX27 after deletion of its PDZ domain. Although the domain involved in binding between GLP-1R and SNX27 is not elucidated, it is interesting to note that a second receptor barcode, formed of sequence determinants or conserved phosphorylation sites, has recently been revealed to dramatically enhance interactions between GPCRs and SNX27 (45).

SNX27 serves as a cargo adaptor for retromer-mediated transport to the cell surface (46), and, accordingly, we found a significant reduction in GLP-1R cell surface recycling after SNX27 knockdown. Intriguingly, despite reduced cell surface levels, GLP-1R signaling remained elevated in MIN6B1 and MIN6B1–SNAP–GLP-1R cells. Concomitantly, we found elevated signaling from internalized receptors, indicating that SNX27 integrates plasma membrane recycling and retromer-mediated GLP-1R signal termination, as seen for other GPCRs such as the parathyroid hormone receptor (47). Direct association of retromer with GLP-1Rs might occur via structural similarity of the VPS26 retromer subunit to β-arrestins (48), perhaps explaining the association between GLP-1R and SNX27 in the absence of a PDZ-binding motif.

Depletion of SNX27 is associated with defective constitutive receptor recycling and increased lysosomal turnover (49,50). The results from MIN6B1–SNAP–GLP-1R cells imply, however, that under mild SNX27 knockdown, sufficient basal levels of GLP-1R are maintained to enable overall incretin-induced cAMP increases, with compensatory mechanisms likely such as increased GLP-1R translation. Indeed, under these conditions, we did not detect a significant decrease in basal levels of SNAP–GLP-1R. However, with more efficient SNX27 knockdown, such as in CHO–SNAP–GLP-1R cells, basal SNAP–GLP-1R levels were significantly reduced, in agreement with continuous missorting of receptors to degradative compartments. As a consequence, in these and in EndoC-βH1 SNX27 shRNA cells, GLP-1R signaling and ISIS were blunted, and elevated endosomal cAMP was no longer detected.

In conclusion, we have identified nine endocytic factors as regulators of ISIS of potential importance for GLP-1R responses in health and diabetes. We show that one of them, HIP1, is required for establishment of plasma membrane incretin responses, whereas SNX1 and SNX27 control GLP-1R recycling and turnover, determining overall GLP-1R outputs. Agents that affect interactions between these trafficking regulators and the GLP-1R may in the future provide interesting new targets to improve the efficacy of incretin-based type 2 diabetes therapies.

Acknowledgments. MIN6B1 cells were provided by Philippe Halban (University of Geneva, Geneva, Switzerland) with permission from Jun-ichi Miyazaki (University of Osaka) who produced the maternal MIN6 cell line. Human islets from Oxford were isolated within the Diabetes Research & Wellness Foundation Human Islet Isolation Facility. This was supported by the National Institute for Health Research Oxford Biomedical Research Centre and by a grant from JDRF. Human islets from Milan and Geneva were provided through the European Consortium for Islet Transplantation, sponsored by JDRF (1-RSC-2014-90-I-X and 1-RSC-2014-100-I-X, respectively). Human islets from Edmonton were provided by the Clinical Islet Transplant Program and the Alberta Diabetes Institute IsletCore at the University of Alberta with the assistance of the Human Organ Procurement and Exchange program, Trillium Gift of Life Network, and other Canadian organ procurement organizations. The authors thank Dr. Tatsuya Kin and Doug O'Gorman (Clinical Islet Isolation Laboratory, University of Alberta) for additional supply of human research islets.

Funding. A.M.J.S. holds a Canada Research Chair in Regenerative Medicine and Transplantation Surgery from the Canada Research Council. G.A.R. was supported by a Wellcome Trust Senior Investigator Award (WT098424AIA), Medical Research Council (MRC) Programme grants (MR/J0003042/1, MR/L020149/1), Experimental Challenge grant (DIVA, MR/L02036X/1), Biotechnology and Biological Sciences Research Council (BB/J015873/1), MRC (MR/N00275X/1), Diabetes UK (BDA/11/0004210, BDA/15/0005275, BDA16/0005485), Imperial Confidence in Concept grants, and a Royal Society Wolfson Research Merit Award. A.T. was supported by a MRC Project grant (MR/M012646/1) and a Diabetes UK Early-Career Small grant (16/0005441).

Duality of Interest. No potential conflicts of interest relevant to this article were reported.

Author Contributions. T.B. performed most experiments and analyzed data. N.K. and P.C.D. performed some experiments. B.J., S.R.B., and I.R.C. contributed novel reagents or technically. P.C. contributed to the calcium flux experiments in human islets. D.B., L.P., P.M., P.R.J., and A.M.J.S. supplied human islets. G.A.R. contributed to the study design, with reagents, and in writing the manuscript. A.T. conceived the study and designed the experiments, performed the confocal and electron microscopy experiments, analyzed the data, and wrote the paper. All authors reviewed and approved the paper. A.T. is the guarantor of this work and, as such, had full access to all the data in the study and takes responsibility for the integrity of the data and the accuracy of the data analysis.

References

1. Willard FS, Sloop KW. Physiology and emerging biochemistry of the glucagon-like peptide-1 receptor. Exp Diabetes Res 2012;2012:470851

2. Drake MT, Shenoy SK, Lefkowitz RJ. Trafficking of G protein-coupled receptors. Circ Res 2006;99:570–582

3. Roed SN, Wismann P, Underwood CR, et al. Real-time trafficking and signaling of the glucagon-like peptide-1 receptor. Mol Cell Endocrinol 2014;382:938–949

4. Hanyaloglu AC, von Zastrow M. Regulation of GPCRs by endocytic membrane trafficking and its potential implications. Annu Rev Pharmacol Toxicol 2008;48:537–568
5. Premont RT, Gainetdinov RR. Physiological roles of G protein-coupled receptor kinases and arrestins. Annu Rev Physiol 2007;69:511–534
6. Xiao K, Sun J, Kim J, et al. Global phosphorylation analysis of beta-arrestin-mediated signaling downstream of a seven transmembrane receptor (7TMR). Proc Natl Acad Sci U S A 2010;107:15299–15304
7. Jean-Alphonse F, Bowersox S, Chen S, Beard G, Puthenveedu MA, Hanyaloglu AC. Spatially restricted G protein-coupled receptor activity via divergent endocytic compartments. J Biol Chem 2014;289:3960–3977
8. Marchese A, Trejo J. Ubiquitin-dependent regulation of G protein-coupled receptor trafficking and signaling. Cell Signal 2013;25:707–716
9. Dores MR, Trejo J. Atypical regulation of G protein-coupled receptor intracellular trafficking by ubiquitination. Curr Opin Cell Biol 2014;27:44–50
10. Romero G, von Zastrow M, Friedman PA. Role of PDZ proteins in regulating trafficking, signaling, and function of GPCRs: means, motif, and opportunity. Adv Pharmacol 2011;62:279–314
11. Bhattacharya M, Babwah AV, Ferguson SS. Small GTP-binding protein-coupled receptors. Biochem Soc Trans 2004;32:1040–1044
12. van Weering JR, Verkade P, Cullen PJ. SNX-BAR proteins in phosphoinositide-mediated, tubular-based endosomal sorting. Semin Cell Dev Biol 2010;21:371–380
13. Vilardaga JP, Jean-Alphonse FG, Gardella TJ. Endosomal generation of cAMP in GPCR signaling. Nat Chem Biol 2014;10:700–706
14. van der Burg JM, Björkqvist M, Brundin P. Beyond the brain: widespread pathology in Huntington's disease. Lancet Neurol 2009;8:765–774
15. Abubakar YS, Zheng W, Olsson S, Zhou J. Updated insight into the physiological and pathological roles of the retromer complex. Int J Mol Sci 2017;18:1601
16. Miyazaki J, Araki K, Yamato E, et al. Establishment of a pancreatic beta cell line that retains glucose-inducible insulin secretion: special reference to expression of glucose transporter isoforms. Endocrinology 1990;127:126–132
17. Lilla V, Webb G, Rickenbach K, et al. Differential gene expression in well-regulated and dysregulated pancreatic beta-cell (MIN6) sublines. Endocrinology 2003;144:1368–1379
18. Gurgul-Convey E, Kaminski MT, Lenzen S. Physiological characterization of the human EndoC-βH1 β-cell line. Biochem Biophys Res Commun 2015;464:13–19
19. Hodson DJ, Mitchell RK, Bellomo EA, et al. Lipotoxicity disrupts incretin-regulated human β cell connectivity. J Clin Invest 2013;123:4182–4194
20. Everett KL, Cooper DM. An improved targeted cAMP sensor to study the regulation of adenylyl cyclase 8 by Ca2+ entry through voltage-gated channels. PLoS One 2013;8:e75942
21. Jaensch N, Corrêa IR Jr., Watanabe R. Stable cell surface expression of GPI-anchored proteins, but not intracellular transport, depends on their fatty acid structure. Traffic 2014;15:1305–1329
22. Tomas A, Futter C, Moss SE. Annexin 11 is required for midbody formation and completion of the terminal phase of cytokinesis. J Cell Biol 2004;165:813–822
23. Martinez-Sanchez A, Pullen TJ, Chabosseau P, et al. Disallowance of Acot7 in β-cells is required for normal glucose tolerance and insulin secretion. Diabetes 2016;65:1268–1282
24. Hodson DJ, Tarasov AI, Gimeno Brias S, et al. Incretin-modulated beta cell energetics in intact islets of Langerhans. Mol Endocrinol 2014;28:860–871
25. Jonas KC, Fanelli F, Huhtaniemi IT, Hanyaloglu AC. Single molecule analysis of functionally asymmetric G protein-coupled receptor (GPCR) oligomers reveals diverse spatial and structural assemblies. J Biol Chem 2015;290:3875–3892
26. Talbot J, Joly E, Prentki M, Buteau J. β-arrestin1-mediated recruitment of c-Src underlies the proliferative action of glucagon-like peptide-1 in pancreatic β INS832/13 cells. Mol Cell Endocrinol 2012;364:65–70
27. Chan AS, Clairfeuille T, Landao-Bassonga E, et al. Sorting nexin 27 couples PTHR trafficking to retromer for signal regulation in osteoblasts during bone growth. Mol Biol Cell 2016;27:1367–1382
28. Hussain NK, Diering GH, Sole J, Anggono V, Huganir RL. Sorting nexin 27 regulates basal and activity-dependent trafficking of AMPARs. Proc Natl Acad Sci U S A 2014;111:11840–11845
29. Wang X, Zhao Y, Zhang X, et al. Loss of sorting nexin 27 contributes to excitatory synaptic dysfunction by modulating glutamate receptor recycling in Down's syndrome. Nat Med 2013;19:473–480
30. McMahon HT, Boucrot E. Molecular mechanism and physiological functions of clathrin-mediated endocytosis. Nat Rev Mol Cell Biol 2011;12:517–533
31. Huang X, Dai FF, Gaisano G, et al. The identification of novel proteins that interact with the GLP-1 receptor and restrain its activity. Mol Endocrinol 2013;27:1550–1563
32. Roed SN, Nøhr AC, Wismann P, et al. Functional consequences of glucagon-like peptide-1 receptor cross-talk and trafficking. J Biol Chem 2015;290:1233–1243
33. Zhu L, Almaça J, Dadi PK, et al. β-Arrestin-2 is an essential regulator of pancreatic β-cell function under physiological and pathophysiological conditions. Nat Commun 2017;8:14295
34. Singaraja RR, Huang K, Sanders SS, et al. Altered palmitoylation and neuropathological deficits in mice lacking HIP14. Hum Mol Genet 2011;20:3899–3909
35. Kennedy JE, Marchese A. Regulation of GPCR trafficking by ubiquitin. Prog Mol Biol Transl Sci 2015;132:15–38
36. Moser E, Kargl J, Whistler JL, Waldhoer M, Tschische P. G protein-coupled receptor-associated sorting protein 1 regulates the postendocytic sorting of seven-transmembrane-spanning G protein-coupled receptors. Pharmacology 2010;86:22–29
37. Metzler M, Legendre-Guillemin V, Gan L, et al. HIP1 functions in clathrin-mediated endocytosis through binding to clathrin and adaptor protein 2. J Biol Chem 2001;276:39271–39276
38. Rao DS, Bradley SV, Kumar PD, et al. Altered receptor trafficking in Huntingtin interacting protein 1-transformed cells. Cancer Cell 2003;3:471–482
39. Fridlyand LE, Philipson LH. Pancreatic beta cell G-protein coupled receptors and second messenger interactions: a systems biology computational analysis. PLoS One 2016;11:e0152869
40. Janssens J, Etienne H, Idriss S, Azmi A, Martin B, Maudsley S. Systems-level G protein-coupled receptor therapy across a neurodegenerative continuum by the GLP-1 receptor system. Front Endocrinol (Lausanne) 2014;5:142
41. Heydorn A, Søndergaard BP, Ersbøll B, et al. A library of 7TM receptor C-terminal tails. Interactions with the proposed post-endocytic sorting proteins ERM-binding phosphoprotein 50 (EBP50), N-ethylmaleimide-sensitive factor (NSF), sorting nexin 1 (SNX1), and G protein-coupled receptor-associated sorting protein (GASP). J Biol Chem 2004;279:54291–54303
42. Gullapalli A, Wolfe BL, Griffin CT, Magnuson T, Trejo J. An essential role for SNX1 in lysosomal sorting of protease-activated receptor-1: evidence for retromer-, Hrs-, and Tsg101-independent functions of sorting nexins. Mol Biol Cell 2006;17:1228–1238
43. Nisar S, Kelly E, Cullen PJ, Mundell SJ. Regulation of P2Y1 receptor traffic by sorting nexin 1 is retromer independent. Traffic 2010;11:508–519
44. Gallon M, Cullen PJ. Retromer and sorting nexins in endosomal sorting. Biochem Soc Trans 2015;43:33–47
45. Clairfeuille T, Mas C, Chan AS, et al. A molecular code for endosomal recycling of phosphorylated cargos by the SNX27-retromer complex. Nat Struct Mol Biol 2016;23:921–932
46. Temkin P, Lauffer B, Jäger S, Cimermancic P, Krogan NJ, von Zastrow M. SNX27 mediates retromer tubule entry and endosome-to-plasma membrane trafficking of signalling receptors. Nat Cell Biol 2011;13:715–721
47. McGarvey JC, Xiao K, Bowman SL, et al. Actin-sorting nexin 27 (SNX27)-retromer complex mediates rapid parathyroid hormone receptor recycling. J Biol Chem 2016;291:10986–11002
48. Shi H, Rojas R, Bonifacino JS, Hurley JH. The retromer subunit Vps26 has an arrestin fold and binds Vps35 through its C-terminal domain. Nat Struct Mol Biol 2006;13:540–548
49. Steinberg F, Gallon M, Winfield M, et al. A global analysis of SNX27-retromer assembly and cargo specificity reveals a function in glucose and metal ion transport. Nat Cell Biol 2013;15:461–471
50. Lauffer BE, Melero C, Temkin P, et al. SNX27 mediates PDZ-directed sorting from endosomes to the plasma membrane. J Cell Biol 2010;190:565–574